IEEE Access
Multidisciplinary | Rapid Review | Open Access Journal

Received August 14, 2020, accepted September 5, 2020, date of publication September 10, 2020,
date of current version September 23, 2020.

Digital Object Identifier 10.1109/ACCESS.2020.3023306

Fault Diagnosis of Rolling Bearing Based on GA-VMD and Improved WOA-LSSVM

JUNNING LI, WUGE CHEN, KA HAN, AND QIAN WANG
School of Mechatronic Engineering, Xi'an Technological University, Xi'an 710021, China

Corresponding author: Junning Li (junningli@outlook.com)

This work was supported in part by the Program of the State Key Laboratory of Mechanical Transmissions under Grant SKLMT-KFKT-201808, in part by the National Natural Science Foundation of China under Grant 51505361, in part by the Innovative Talents Promotion Plan in Shaanxi Province under Grant 2017KJXX-58, and in part by the Natural Science Basic Research Program of Shaanxi under Grant 2020JM-564.

ABSTRACT To improve the fault identification accuracy of rolling bearings due to the problems of parameter optimization and low convergence accuracy, a novel fault diagnosis method for rolling bearings combining wavelet threshold de-noising, genetic algorithm optimization variational mode decomposition (GA-VMD) and the whale optimization algorithm based on the von Neumann topology optimization least squares support vector machine (VNWOA-LSSVM) is proposed in this manuscript. First, wavelet threshold de-noising is used to preprocess the vibration signal to reduce the noise and improve the signal-to-noise ratio (SNR). Second, a genetic algorithm (GA) is utilized to optimize the parameters of variational mode decomposition (VMD), and optimized VMD is adopted to extract the fault feature information. The VNWOA-LSSVM fault diagnosis model is built to train and identify the fault feature vectors. The proposed method is validated by experimental data. The results show that this method can not only effectively diagnose various damage positions and extents of rolling bearings but also has good identification accuracy.

INDEX TERMS Wavelet threshold de-noising, genetic algorithm, variational modal decomposition, von Neumann topology, rolling bearing.

I. INTRODUCTION

As an important widely used component, rolling bearings impact the stable operation of mechanical equipment [1]. Rolling bearings directly affect the service performance of the whole mechanical equipment, and so it is of great significance to carry out fault diagnosis research on rolling bearings. For fault diagnosis of rolling bearings, the most critical thing is to accurately extract the faulty feature information of the rolling bearings, and adopt this information to analyze the running status of the rolling bearings.

Fault diagnosis of rolling bearings is mostly represented using the time-domain or frequency-domain, and the commonly used fault diagnosis methods included the Wavelet transform, Fourier transform, Hilbert transform, etc. [2]–[4]. However, when a fault occurs, the signal is mostly nonlinear and non-stationary. It is difficult to extract the effective component of fault feature information from a signal in the time-domain or frequency-domain. Therefore, a signal processing method combining the time-domain and the frequency-domain is produced. Huang *et al.* [5] proposed Empirical mode decomposition (EMD) and applied it in time-frequency domain analysis. EMD is widely used in the processing of different signals, and it automatically decomposes signals into a series of modal components from high frequency to low frequency. Yu *et al.* [6] applied the EMD and Hilbert spectrum to fault diagnosis of rolling bearings and compared the method with the envelope spectrum to prove that the proposed method can effectively diagnose rolling bearings. To realize the diagnosis of different fault types of rolling bearings, Ali *et al.* [7] proposed a fault diagnosis method combining EMD and energy entropy. The vibration signal of the bearing was decomposed by EMD to obtain the modal component, and then the energy entropy of each modal component was calculated. Cai *et al.* [8] introduced a fault diagnosis method for rail transit rolling bearings based on the combination of EMD and the genetic neural network adaptive enhancement. The EMD method has certain advantages, but it has some problems such as mode aliasing and endpoint

The associate editor coordinating the review of this manuscript and approving it for publication was Ruqiang Yan.

effects [9]–[11]. Gaci [12] proposed the total average ensemble empirical mode decomposition (EEMD) to eliminate the influence of noise on a vibration signal by adding Gaussian white noise. To solve the problem of the unknown type and characteristic frequency of rolling bearings in actual engineering applications, Yang *et al.* [13] adopted the EEMD and stochastic resonance technology, established the cut-off frequency criterion and spectral amplification factor to select the effective component and verified the effectiveness of the proposed method through three rolling bearings experiments with different fault types. To improve the efficiency and accuracy of fault diagnosis, Zou *et al.* [14] combined signal preprocessing, EEMD and the long-short-term memory (LSTM) algorithm to implement fault diagnosis of rolling bearings. Although EEMD overcomes the modal aliasing problem of EMD, it still has the endpoint effects [14]. Sun *et al.* [15], Tian *et al.* [16] proposed local characteristic-scale decomposition (LCD), which could adaptively decompose complex multi-component signals into a series of single-component intrinsic scale components and effectively extract fault feature information. Luo *et al.* [17] adopted singular value decomposition and the LCD algorithm to extract the feature information, and then combined the artificial neural net and mean impact value to select more accurate fault feature information of rolling bearings. Ao *et al.* [18] utilized LCD to decompose the vibration signal into multiple intrinsic scale components, and applied the support vector machine (SVM) fault diagnosis model based on the artificial chemical reaction optimization algorithm to diagnose fault. However, LCD has unreasonable definitions of the mean curve and modal aliasing in the decomposition process. VMD was proposed to search for the optimal solution of the variational model and determine the frequency center and the bandwidth by Dragomiretshiy and Zosso [19]. Wu *et al.* [20] adopted the VMD algorithm to decompose the vibration signal to obtain multiple sets of modal components, and then introduced the kernel function joint approximate diagonalization of eigenmatrices (KJADE) to calculate the features of each modal component in the time-domain, frequency-domain and time-frequency domain. Ren *et al.* [21] proposed VMD to decompose vibration data, and combined the multi-scale permutation entropy and feature transfer learning to extract the feature information.

Although the VMD method can adaptively achieve the frequency division of the vibration signal, however, its decomposition results are heavily restricted to the selection of the modal number k and the penalty parameter α. Therefore, the parameter setting of VMD becomes an urgent problem to be solved. With the emergence of intelligent algorithms, more researchers combined intelligent algorithms with parameter optimization. Gu *et al.* [22] introduced the gray wolf algorithm to optimize the optimal parameters of VMD, and used the minimum average envelope entropy as the fitness value. Li *et al.* [23] introduced the principle of the maximum kurtosis to optimize the parameters of VMD and obtain the best α and k parameters.

The essence of fault diagnosis is pattern identification [24]. With the continuous development of machine learning and deep learning in recent years, fault features have been analyzed by using neural networks [25], support vector machines [26], [27], shallow model, artificial neural networks, deep learning [28] and the hidden Markov chain [29], and then classification model is established to realize intelligent classification of fault patterns in rolling bearing. Many scholars applied machine learning in fault classification and diagnosis [28]. Artificial neural networks are the abstraction of human brain neural network. Islam and Kim [30] used a discrete wavelet packet transform method to train convolutional neural network (CNN) in bearing fault diagnosis. Li *et al.* [31] proposed a precise diagnosis method for rotating machinery based on the combination of Deep Belief Network (DBN) and 1D-CNN. As a classical machine learning algorithm, the SVM is widely used owing to its simplicity. The SVM is a small-sample learning method that converts low-dimensional linear non-separable data into high-dimensional linear separable data [32]. The classification accuracy of the SVM is greatly affected by the selection of the penalty parameter C and kernel parameter g, and the manual selection is inefficient and has difficulties finding the optimal parameter. Currently, there are many intelligent optimization algorithms, including the WOA, particle swarm optimization (PSO), ant colony optimization (ACO), the gray wolf optimizer (GWO), the firefly algorithm (FA), the GA, etc. The combination of intelligent optimization algorithms and the SVM could be used to determine its optimal parameters. Wang *et al.* [33] presented the GWO algorithm to optimize the SVM and applied it to fault diagnosis of rolling bearings. Qiao *et al.* [34] used a quantum genetic algorithm to optimize the parameters of the SVM. The intelligent optimization algorithm has some advantages, but it still has some disadvantages. For example, the WOA has a slow convergence speed and it easily falls into the local optimum when dealing with complex optimization problems. The GA is prone to the premature convergence phenomenon. Therefore, the structure of an intelligent algorithm needs to be reasonably optimized. To solve the defects of the WOA, Wu *et al.* [20] introduced the von Neumann topology to improve the WOA, and the results showed that the improved algorithm had a stronger optimization ability and faster convergence speed. Vijayanand and Devaraj [35] combined genetic algorithm operators with the WOA and improved the search space of the WOA by using crossover operators to avoid it falling into the local optimal solution. Zhang and Liu [36] proposed the WOA with the Lamarckian learning method, which adopted point set theory to initialize the population parameters and used the evolutionary theory of Lamarck to select the individuals with more development potential to perform the local search. As an improvement to the SVM, the LSSVM transforms the inequality constraints of the SVM into equality constraints, which increases the solving speed. Gao *et al.* [37] optimized the parameters in the LSSVM with PSO and a 10-fold cross-validation

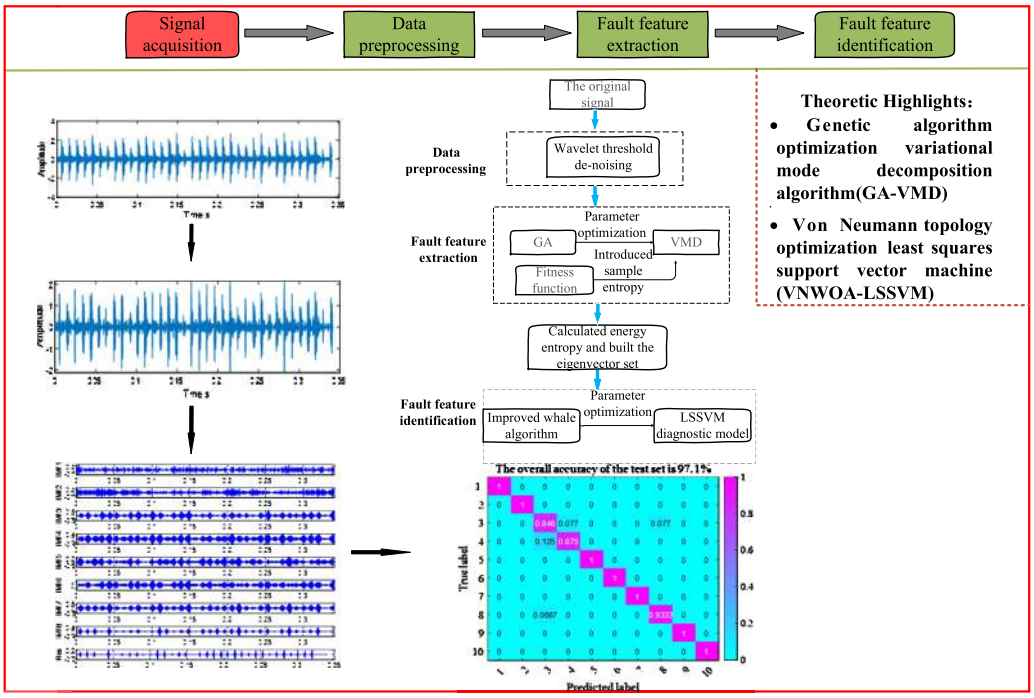

FIGURE 1. Overall flowchart of this research.

method, and then used it to update the fault diagnosis model. Liu *et al.* [38] adopted LSSVM model optimized by quantum particle swarm optimization (QPSO) algorithm to perform training and identification fault feature of rolling bearing.

To solve the difficult parameter optimization problem in VMD and the low convergence accuracy of the WOA, in this manuscript, a novel fault diagnosis method of rolling bearings based on wavelet threshold de-noising, the GA-VMD energy entropy and the VNWOA-LSSVM algorithm is proposed.

II. MATERIALS AND METHODS

In this manuscript, fault diagnosis of rolling bearings is carried out from three aspects: data preprocessing, fault feature extraction and fault feature identification. The overall flowchart is shown in Fig. 1.

A. DATA PREPROCESSING

The collected vibration signal of a rolling bearing contains different extents of background noise. To accurately extract the feature information, it is necessary that reduce the interference of the background noise on the vibration signal. Signal de-noising methods include wavelet de-noising, singular value decomposition de-noising, filter de-noising and empirical mode decomposition de-noising. Among them, wavelet de-noising is widely used due to its good adaptability and fast decomposition speed. Therefore, the wavelet threshold de-noising method is adopted in this manuscript, and the vibration signal is denoised by using the db5 wavelet, which can satisfy the key properties better than others [39]. Several trials have been conducted to identify the wavelet transforms that highly suitable to the present problem, and db 5 is identified as the best choice [40]. The three main steps of wavelet de-noising include wavelet decomposition, threshold quantization and reconstruction of wavelet signal [41].

There are two common threshold functions for wavelet threshold de-noising methods: the soft threshold and the hard threshold. The hard threshold function can produce the Gibbs effect to a certain extent while the soft threshold function can better satisfy the signal adaptability. The soft threshold function is expressed as (1). The method of wavelet soft-threshold de-noising proposed by Chen *et al.* [41]. The threshold is obtained by wden, and then the threshold parameters of the noise layer are automatically adjusted according to the wavelet coefficients of the first layer. The thresholding is applied to all wavelet coefficients.

$$\omega_\lambda = \begin{cases} [sign\,(\omega)]\,(|\omega| - \lambda)\,, & |\omega| \geq \lambda \\ 0, & |\omega| < \lambda \end{cases} \tag{1}$$

where ω represents wavelet coefficients, ω_λ denotes the coefficient after applying the threshold, λ is threshold.

Wden is a function in MATLAB Wavelet Toolbox, which can be used to wavelet threshold de-noising. Wden function uses an N-level wavelet decomposition of signal using the specified orthogonal or biorthogonal wavelet name to obtain the wavelet coefficients, and wden function is shown in (2).

$$xd = wden\,(x, tptr, sorh, scal, n, wname) \tag{2}$$

where, xd represents the signal after de-noising obtained by wavelet threshold quantization; x denotes the input original signal; tptr is the threshold selection rule specified; sorh

represents the selection mode of threshold; n is the number of decomposed layers; wname indicates the wavelet basis function.

B. FAULT FEATURE EXTRACTION

1) GENETIC ALGORITHM OPTIMIZATION OF VMD

The VMD algorithm transforms the decomposition process of the signal into the optimal solution problem of the variational mode to realize the frequency band separation of the signal. The VMD algorithm converts the vibration signal into a series of modal components u_k with limited bandwidth, and requires each modal component u_k to revolve around a central frequency w_k. The VMD constraint condition is that the sum of all modes is equal to the original signal, and the sum of the estimated bandwidth of each mode is the minimum. Then, the mathematical expression of the variational model is shown in (3).

$$\begin{cases} \min \left\{ \sum_k \left\| \partial t \left[\left(\delta(t) + \frac{j}{\pi t} \right) * u_k(t) \right] e^{-j\omega_k t} \right\|_2^2 \right\} \\ s.t. \sum_k u_k = f \end{cases} \tag{3}$$

To solve the optimal solution of the constraint variable component problem in (3), the Lagrange punishment operator L and secondary penalty factor α are introduced to transform the constraint variable component problem into a non-constraint problem. The expression is shown in (4), as shown at the bottom of the next page.

The VMD algorithm avoids the modal aliasing in the EMD algorithm, but its decomposition effect is limited by the number of modal decompositions k and the secondary penalty factor α. If k is too small, it will cause under decomposition, which makes it difficult to fully extract the fault information. However, if k is too large, it will cause over decomposition, which causes repeated modalities. If α is too small, the modal component may contain numerous noises; whereas, if α is too large, the vibration signal may be decomposed into two or more modes. Improper selection of the parameters [k, α] will reduce the fault identification accuracy. Therefore, a reasonable set of parameters [k, α] is crucial to the decomposition effect of VMD. With the emergence of intelligent algorithms, more researchers combined intelligent algorithms with VMD parameter optimization. The GA was first proposed by Bagley [35], and the GA is realized by first establishing a reasonable optimal fitness function. In this manuscript, the sample entropy is introduced as the fitness function of the GA. The sample entropy can be used to characterize the irregularity and complexity of the signal and evaluate the signal regularity. The lower the sample entropy is, the higher the signal regularity, that is, the more obvious the periodic signal characteristics of the rolling bearing. With the help of the fitness function, the global search for the objective function value in the solution space is conducted. The expression of the objective function is shown in (5).

$$\langle \alpha, k \rangle = \arg\min \left\{ \frac{1}{k} \sum_{i=1}^{k} H_{en1}(i) \right\} \tag{5}$$

where k and α represent the optimization parameters of VMD, and H_{en1} represents the sample entropy value of each mode. The expression of sample entropy is shown in (6).

$$\begin{cases} H_{en1} = -\ln[A^m(r)/B^m(r)] \\ A^m(r) = \dfrac{1}{N-m} \sum_{i=1}^{N-m} A_i^m(r) \\ A_i^m(r) = \dfrac{1}{N-m-1} A_i \\ B^m(r) = \dfrac{1}{N-m} \sum_{i=1}^{N-m} B_i^m(r) \\ B_i^m(r) = \dfrac{1}{N-m-1} B_i \end{cases} \tag{6}$$

where m is the dimension, and r is the similar tolerance. $B^m(r)$ represents the probability that two sequences match m points under the similar tolerance, and $A^m(r)$ represents the probability that two sequences match m +1 points. $A_i^m(r)$ and $B_i^m(r)$ are defined matching probability, N is the length of the data.

Fig. 2 shows the process of the GA-VMD method. The first thing is to set the initialization range of the parameter [k, α]. After numerous trials, we finally choose a more reasonable range of k in (3, 10) and α in (500, 2000) in this manuscript. The second thing is the initialization of the GA parameters. The GA parameters used in this manuscript similar to reference [43]: The maximum number of iterations is 50, the population size is 10, the crossover probability is 0.8, and the mutation probability is 0.1. Then, a random population is generated. The VMD algorithm parameters [k, α] are optimized, and the sample entropy of each individual is calculated. In addition, GA selection, crossover and mutation are carried out to find the individual with the smallest fitness function value in the population. When it reaches maxgen, the VMD parameter optimization process is completed, and then the best [k, α] value is output.

2) VMD ENERGY ENTROPY

Once a bearing failure occurs, the energy value of the vibration signal will change when the bearing rotates through the damaged area. In addition, the energy entropy of the rolling bearing will also change when different types of damage occur. Therefore, the concept of the VMD energy entropy is introduced in this manuscript.

Through the VMD of the vibration signals x(t) of different fault types, a series of modal components and a residual component are obtained. The energy value $E_1, E_2, E_3, \ldots, E_n$ of each modal component is calculated separately, and the ratio of each modal component to the total component is also calculated. The VMD energy entropy is shown in (7), where E represents the total energy value of the intrinsic mode

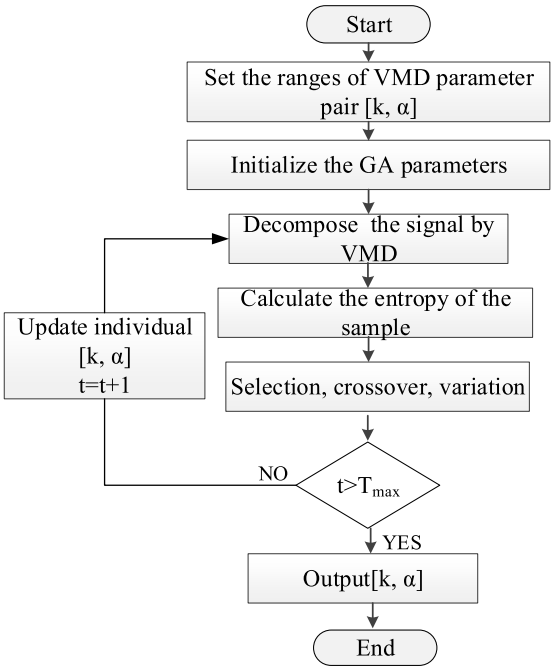

FIGURE 2. Flowchart of the proposed GA-VMD method.

function (IMF). H_{en2} is indicated as the energy entropy value of each mode. p_i is the ratio of the i-th IMF component to the total energy.

$$\begin{cases} H_{\text{en2}}\,(\text{i}) = -\sum_{i=1}^{K} p_i \log_{10}(p_i) \\ p_i = E(\text{i})/E \\ E = \int_{-\infty}^{\infty} |IMF_i|^2\, dt \quad i = 1, 2, \cdots n \end{cases} \tag{7}$$

C. FAULT FEATURE EXTRACTION

1) LSSVM ALGORITHM

The SVM is a basic machine learning method based on statistical theory [44]. Its main idea is to establish an optimal hyperplane to maximize the separation margin between the two types. The LSSVM algorithm is formed by introducing the least-squares linear theory into the SVM, which converts the original SVM inequality constraints into linear equality constraints. Therefore, the problem-solving process is simplified. The optimization objective function is defined as shown in (8).

$$f\,(x) = \text{sgn}\,\{\omega \cdot \phi\,(x) + b\} \tag{8}$$

ω is defined as weight vector, b is deviation vector, $\phi\,(x)$ represents nonlinear mapping function.

The final optimization problem is shown in (9)

$$\begin{cases} \min J\,(\omega, \xi) = \frac{1}{2}\,\|\omega\|^2 + \gamma \sum_{i=1}^{N} \xi_i^2, \\ s.t.\ y_i \left[\omega^T \phi\,(x_i) + b\right] = 1 - \xi_i \\ \quad i = 1, 2, \ldots, N. \end{cases} \tag{9}$$

J is optimized objective function, ξ is error variables, γ represents penalty factor.

To obtain a better classification model, the Lagrange multiplier α_i is introduced. The formula is shown in (10).

$$L\,(\omega, b, \xi, \alpha_i) = J\,(\omega, \xi_i) - \sum_{i=1}^{N} \alpha_i \left\{ y_i \left[\omega^T \phi\,(x_i) + b\right] - 1 + \xi_i \right\} \tag{10}$$

The relevant parameters in (10) are subjected to a partial derivative operation by using the constraints on the Karush-Kuhn-Tucker (KKT) conditions, and the result is set to 0. The expression is shown in (11).

$$\begin{bmatrix} 0 & y^T \\ y & \psi\psi^T + \frac{1}{\gamma} E \end{bmatrix} \begin{bmatrix} b \\ \alpha \end{bmatrix} = \begin{bmatrix} 0 \\ y \end{bmatrix} \tag{11}$$

where $y = [1, 1, \ldots, 1]^{\text{T}}$, E is an identity matrix, $\gamma = [y_1, y_2, \ldots, y_n]^{\text{T}}$, $\alpha = [\alpha_1, \alpha_2, \ldots, \alpha_n]^{\text{T}}$, and $\psi = [\phi\,(x_1), \phi\,(x_2), \ldots, \phi\,(x_n)]^{\text{T}}$. $\phi\,(x_i)$ represents nonlinear mapping function. Finally, the classification model of the LSSVM is as follows:

$$f(x) = \text{sgn}\left[\sum_{i=1}^{n} \alpha_i \text{k}\,(x, x_i) + b\right] \tag{12}$$

$\text{k}\,(x, x_i)$ represents kernel function that satisfying the Mercer condition.

2) IMPROVED WHALE OPTIMIZATION ALGORITHM

The whale optimization algorithm was proposed by Mirjalili and Lewis [45] through studying the hunting behavior of humpback whales. This algorithm is characterized by fewer parameters than other algorithms and has a simple structure and a strong global optimization ability.

When whales surround their prey, it is assumed that the current target prey position is the best in the population. After determining the search agent, each whale in the population also defines this target position as the best search agent. Its position update formulas are as follows:

$$D = \left|CX^*\,(t) - X\,(t)\right| \tag{13}$$

$$X\,(t+1) = X^*\,(t) - AD \tag{14}$$

$$C = 2 \cdot r_2 \tag{15}$$

$$L\,(\{u_k\}, \{\omega_k\}, \lambda) = \alpha \sum_k \left\| \partial_t \left[\left(\delta\,(t) + \frac{j}{\pi t}\right) * u_k\,(t) \right] e^{-j\omega_k t} \right\|_2^2 + \left\| f\,(t) - \sum_k u_k\,(t) \right\|_2^2 + \left\langle \lambda\,(t), f\,(t) - \sum_k u_k\,(t) \right\rangle \tag{4}$$

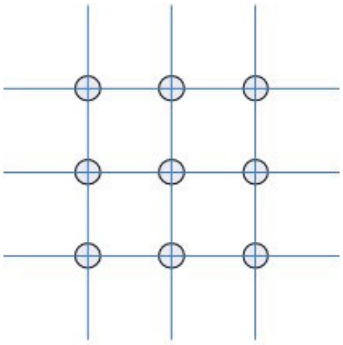

FIGURE 3. Von Neumann topology.

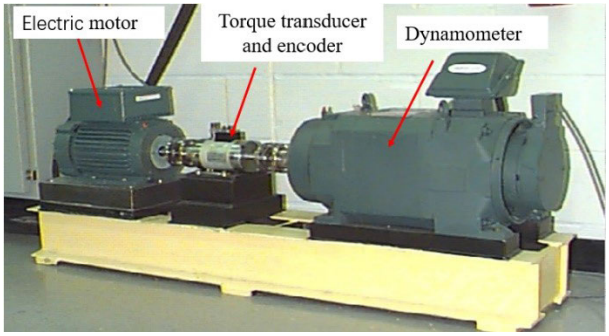

FIGURE 4. Rolling bearing fault simulation experiment system.

$$A = 2ar_1 - a \tag{16}$$

$$a = 2\left(1 - \frac{t}{T_{\max}}\right) \tag{17}$$

In (13)-(17), t represents the current iteration number, and X(t) represents the current whale position. D is indicated as coefficient vector. X*(t) represents the current best whale position, A and C represent coefficients, and T_{max} is the maximum number of iterations. r_1 and r_2 belong to any number in [0, 1], a is represented as a constant and the value decreases linearly from 2 to 0.

When humpback whales hunt prey, they not only need to track their prey with a spiral bubble net, but they also constantly shrink the range to close to the prey. In the range contraction and spiral tracking process, the positions of the whales are continuously updated with a 50% probability. The position formula is shown in (18).

$$X(t+1) = \begin{cases} X^*(t) - \mathrm{A} \cdot \mathrm{D}, & \text{if } \mathrm{p} < 0.5 \\ D' \cdot e^{bl} \cdot \cos(2\pi l) + X^*(t), & \text{if } p \geq 0.5 \end{cases} \tag{18}$$

$D' = |\, X^*(t) - X(t) \,|$ represents the distance between the current whale and the target prey, b defines the shape of the spiral, and l is a random number in [−1, 1].

The whale optimization algorithm has its advantages, but it easily falls into the local optimum and experiences low convergence accuracy in complex optimization problems. Therefore, in this manuscript, the von Neumann topology is introduced to improve the whale algorithm. The von Neumann topology is shown in Fig. 3. There are up, down, left, and right whales around each humpback whale, which forms a grid structure, and then they can exchange information with each other. Each whale finds the optimal solution, which may affect the search mechanism of the surrounding whale individuals and effectively links the interaction of each whale to realize the full use of information between populations, thereby improving its global optimal solution and convergence accuracy.

According to its position update formula, the position update of the whale is affected by the global optimal solution, and the position of the population is updated with it. To enhance the local search ability of the whale algorithm, the midpoint of the global optimal and local optimal positions is taken as the optimal position in the current population. The algorithm considers both the global optimal and the local optimal solutions to better realize the information exchange mechanism among whales. As the number of iterations increases, the global optimal solution and the local optimal solution are constantly approaching and finally return to the original position. The current optimal position calculated using (19).

$$X_i^* = \frac{p_{lbest_i} + G}{2} \tag{19}$$

P_{lbesti} is the optimal position in the local update, G represents the optimal position in the global update.

3) VNWOA-LSSVM

The steps of the LSSVM by using the optimized whale algorithm (VNWOA) are as follows.

Step 1: Use wavelet threshold de-noising to complete the de-noising processing of vibration data, use the improved VMD algorithm to complete the feature extraction of the vibration signal, and calculate the energy entropy to form the feature vector matrix. Divide the sample into the training set and the test set. 190 sets of vibration data under different rolling bearing fault statues are randomly taken as the training sets, and 100 sets are used as the test sets.

Step 2: Initialize the parameters of the whale optimization algorithm. Set the population N as 10 and the maximum number of iterations G_{max} as 50.

Step 3: Determine the network topology of the LSSVM model, and determine the ranges of parameter σ and penalty factor g in [0, 1000].

Step 4: Calculate the fitness function value of each humpback whale and sort the fitness values.

Step 5: Use the von Neumann topology to search for the optimal solution in the neighborhood, complete the information exchange among the populations, search the optimal solution in the neighborhood, and then update its location based on formulas (13), (14), (18) and (19).

Step 6: According to formula (18), whales need to constantly shrink the surrounding area to achieve the best classification accuracy.

TABLE 1. Description of rolling bearing data set.

Bearing type	Fault position	Fault Size(mm)	Fault depth(mm)	Category label
SKF6205	normal	0	0	1
	Inner ring 1	0.1778	0.2794	2
	Inner ring 2	0.3556	0.2794	3
	Inner ring 3	0.5334	0.2794	4
	Outer ring 1	0.1778	0.2794	5
	Outer ring 2	0.3556	0.2794	6
	Outer ring 3	0.5334	0.2794	7
	Rolling element 1	0.1778	0.2794	8
	Rolling element 2	0.3556	0.2794	9
	Rolling element 3	0.5334	0.2794	10

TABLE 2. Comparison of de-noising effects under different wavelet decomposition levels.

Decomposition level	2	3	4	5	6
SNR	41.4878	41.5869	41.2866	41.2836	41.2770
RMSE	0.0227	0.0080	0.0291	0.0299	0.0266

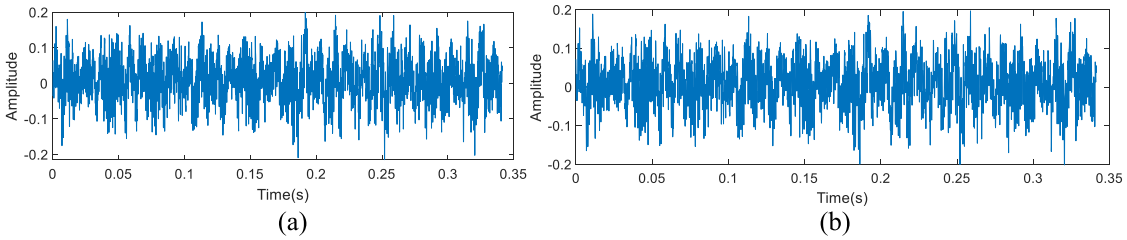

FIGURE 5. Comparison results in the time-domain before and after de-noising of the rolling bearing under normal conditions. (a) original time-domain vibration curve, (b) time-domain vibration curve after de-noising.

Step 7: Repeat steps (5) and (6) until the number of iterations meets G_{max}. Then, the best fitness function value is output to train the LSSVM model, and then the rolling bearing is accurately diagnosed.

III. RESULTS AND DISCUSSION

A. EXPERIMENT SYSTEM

The experimental data in this manuscript are obtained from the bearing database published by Case Western Reserve University, USA. The experiment system consists of a 2 HP motor (left), a torque sensor (middle), a dynamometer (right), and control electronics [46]. The vibration data of the rolling bearing are collected by a 16-channel vibration sensor. The rolling bearing used in the experiment is a SKF6205 deep groove ball bearing. The structure of the experiment system is shown in Fig. 4.

The working conditions used in this test are a speed of 1750r/min, a load of 2HP, and a sampling frequency of 12kHz. The electrical discharge machine (EDM) is used to process the pitting with fault diameters of 0.1778 mm, 0.3556 mm, and 0.5334 mm on the inner ring, outer ring, and the rolling element of the rolling bearing, respectively, which is done to simulate different extents of damage to the rolling bearing. A total of 10 samples are analyzed, and there are 29 groups of data under different damage types. The sample length of each group of vibration data is 4096. 190 groups are randomly selected for the training set and 100 groups are selected for the test sets. The data storage format is a .mat file. The specific sample data set is shown in table 1.

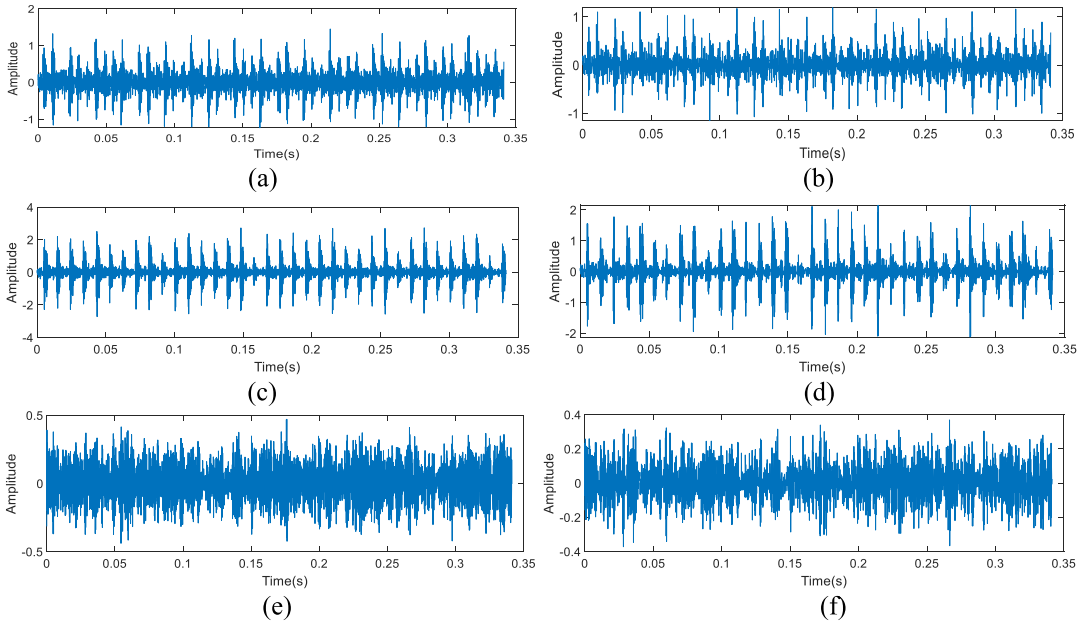

FIGURE 6. Comparison results in the time-domain before and after de-noising of different damaged parts of the rolling bearing with a fault size of 0.1778 mm. (a) original time-domain curve of the inner ring, (b) original time-domain curve of the inner ring after de-noising, (c) original time-domain curve of the outer ring, (d) original time-domain curve of the outer ring after de-noising, (e) original time-domain curve of the rolling element, and (f) original time-domain curve of the rolling element after de-noising.

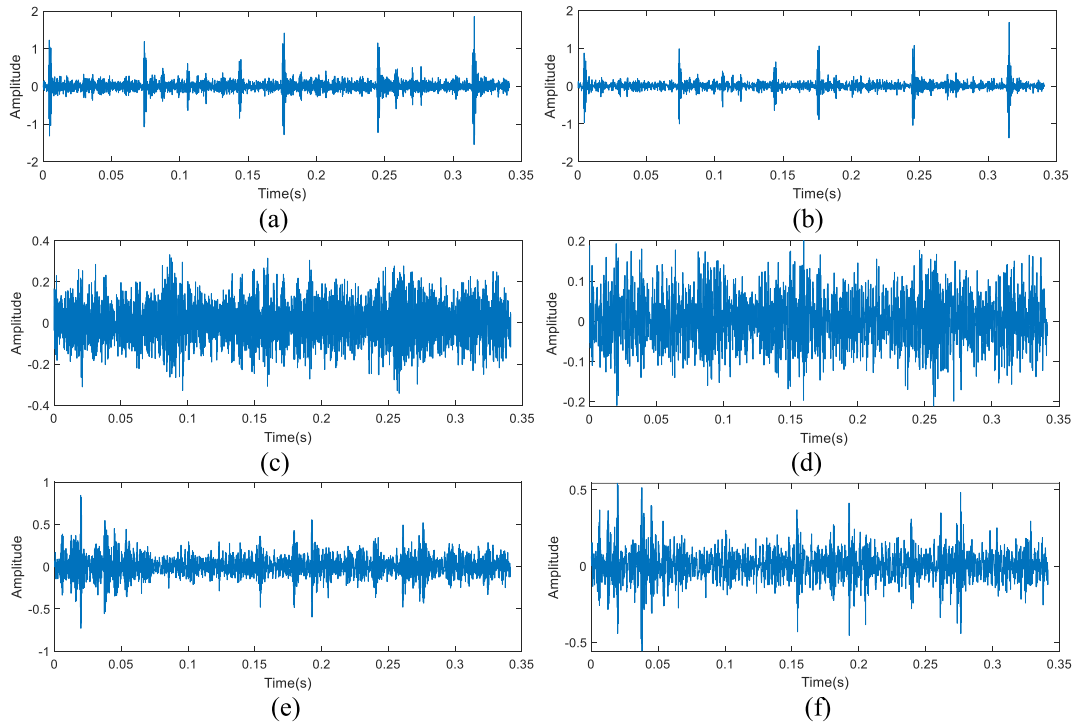

FIGURE 7. Comparison results of the time-domain before and after de-noising of different damaged parts of the rolling bearing with a fault size of 0.3556 mm. (a) original time-domain curve of the inner ring, (b) original time-domain curve of the inner ring after de-noising, (c) original time-domain curve of the outer ring, (d) original time-domain curve of the outer ring after de-noising, (e) original time-domain curve of the rolling element, and (f) original time-domain curve of the rolling element after de-noising.

B. RESULTS AND ANALYSIS

Different decomposition levels based on wavelet basis db5 under normal conditions are tested and listed in Table 2, it shows that the best number of composition level with SNR and RMSE is level 3. De-noising processing of each group of vibration data is performed, and the db5 wavelet is

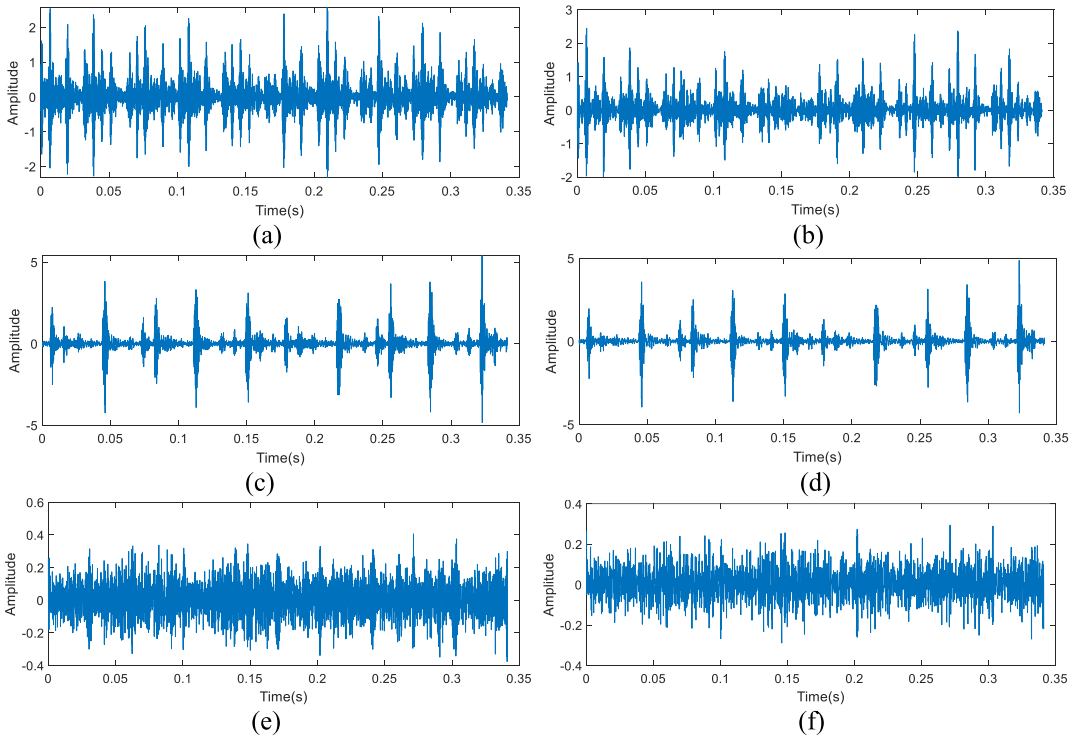

FIGURE 8. Comparison results of the time-domain before and after the de-noising of different damaged parts of the rolling bearing with a fault size of 0.5334 mm. (a) original time-domain curve of the inner ring, (b) original time-domain curve of the inner ring after de-noising, (c) original time-domain curve of the outer ring, (d) original time-domain curve of the outer ring after de-noising, (e) original time-domain curve of the rolling element, and (f) original time-domain curve of the rolling element after de-noising.

utilized to perform three-layer decomposition. Fig. 5 shows the time-domain vibration curve of the rolling bearing under normal operating conditions. Figs. 6, 7, and 8 are the original vibration curves and the vibration curves after the wavelet threshold de-noising of the rolling bearing under different extents and types of damage. By comparing the time-domain curves before and after de-noising, it is found that the vibration data before de-noising is large and contains many burrs. After de-noising, the vibration amplitude is greatly improved, and the burrs are also well suppressed, which achieves the purpose of de-noising to some extent.

Taking the fault size of 0.1778 mm as an example, wavelet threshold de-noising and orthogonal matching pursuit (OMP) de-noising are performed, respectively. The comparison results are shown in table 3. The two indicators of the SNR and root mean square error (RMSE) are adopted to evaluate the de-noising effects of the two methods.

It can be seen from table 3 that after comparing the two de-noising methods, it is found that the SNRs and RMSEs of the wavelet threshold after de-noising are better than those of OMP, and the results show that wavelet threshold de-noising has a better effect. Therefore, the influence of the background noise on the vibration signal of the rolling bearing is weakened, which can be useful for the subsequent extraction of fault features.

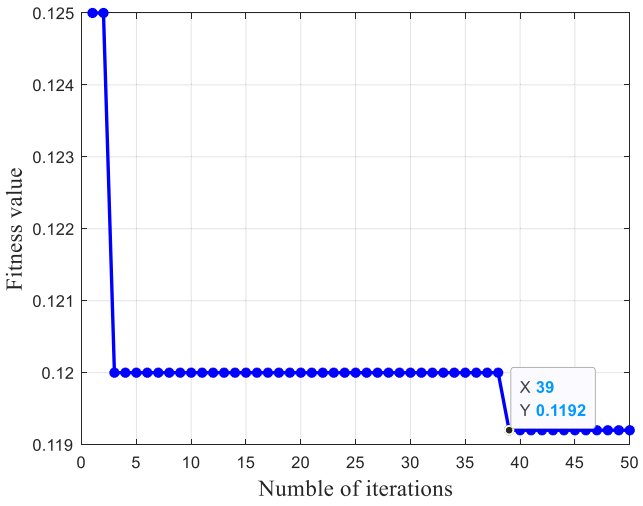

FIGURE 9. Optimized VMD curve with the genetic algorithm.

After wavelet threshold de-noising, the improved VMD algorithm is adopted to extract the fault feature of the vibration signal. Taking the fault size of 0.1778 mm of the outer ring as an example, the GA is utilized to optimize the parameters of the VMD algorithm.

Fig. 9 is the fitness curve of the individual minimum sample entropy value as the number of iterations increases in the GA optimization process. It can be seen from the

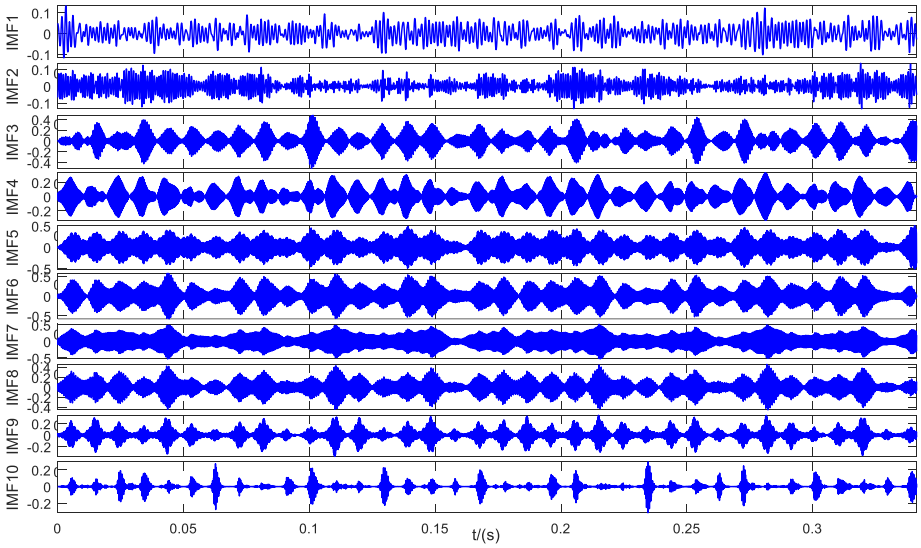

FIGURE 10. VMD decomposition curves after optimization.

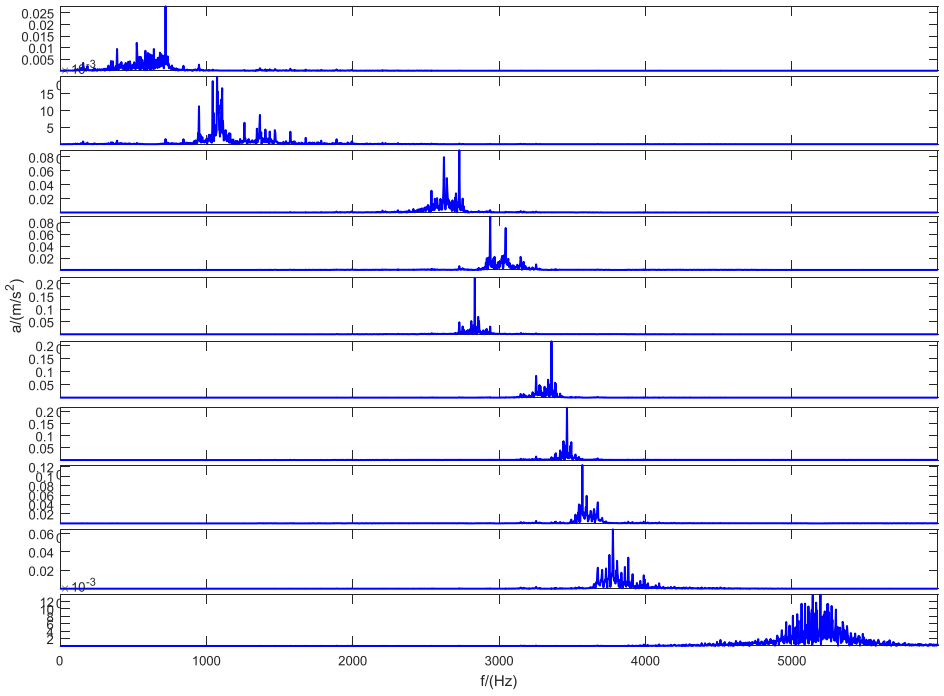

FIGURE 11. Signal spectrum after VMD processing.

figure that the fitness function value has a minimum value of 0.1192 at the 39th iteration. When the number of iterations reaches 50, the optimization process is completed, and the optimal parameters [k, α] are [10, 957]. The VMD is reset according to the optimal parameters [k, α], and then 10 modal components are obtained by using the optimized VMD.

Fig. 11 is the signal spectrum obtained by the optimized VMD. From the spectrum diagram, the fault characteristic frequency of the outer ring is not found, and so envelope spectrum analysis is performed. Fig. 12 shows the envelope spectrum of the outer ring. In this envelope spectrum, the characteristic frequency value of the outer ring is 105.5 Hz, and the spectral amplitude at the f_i-$3f_i$ doubling frequency is very prominent, indicating that the feature information is effectively extracted.

In table 4, GA algorithm is used to optimize VMD algorithm under different fault status of rolling bearings to obtain the best parameters k and α, and then VMD algorithm parameters are set according to the best parameters in the table 4. The vibration signals of different damage positions and

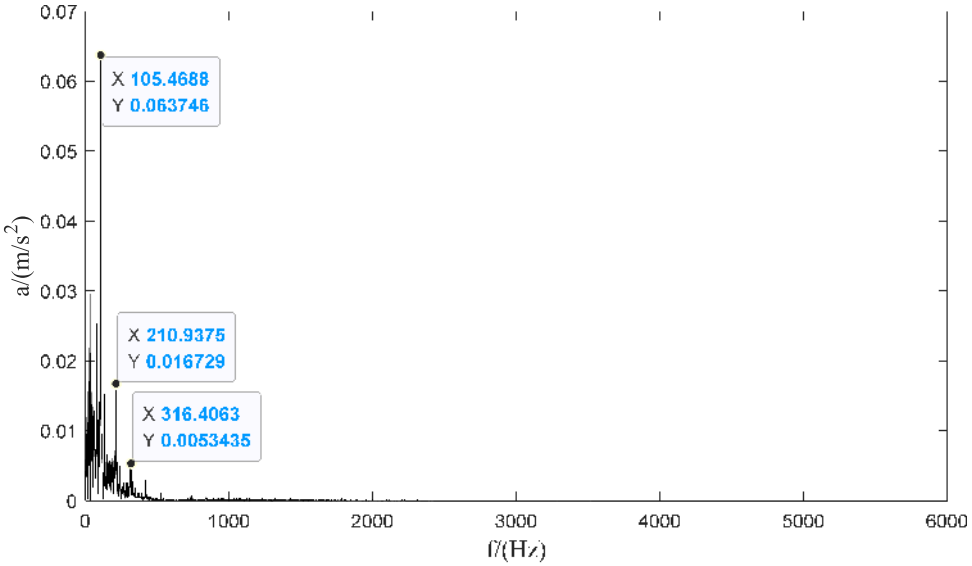

FIGURE 12. Envelope spectrum of modal components.

TABLE 3. Comparison of the de-noising effect.

	wavelet threshold de-noising		OMP	
Bearing status	SNR	RMSE	SNR	RMSE
Inner ring	15.8709	0.1129	9.3055	0.3884
Outer ring	27.2286	0.1271	9.6889	0.7061
Rolling element	5.8988	0.1152	8.5717	0.8886
Normal conditions	41.5869	0.0080	5.4545	0.0839

TABLE 4. Optimization parameters obtained by using the GA.

Bearing status	normal	Inner ring 1	Inner ring 2	Inner ring 3	Outer ring 1	Outer ring 2	Outer ring 3	Rolling element 1	Rolling element 2	Rolling element 3
k	9	10	10	10	10	9	8	9	9	10
α	1963	1715	815	833	957	1363	551	1933	1942	1831

extents of rolling bearings are decomposed by the VMD algorithm after optimized parameter, and the energy entropy of each modal component is calculated.

Table 5 shows the partial energy entropy of the first 6 modal components under different fault statuses. A total of 290*6 energy entropy values can be obtained by using the GA-VMD method.

Based on the fault feature extraction with the wavelet threshold de-noising and improved VMD algorithm, the VNWOA algorithm is used to optimize the LSSVM model to diagnosis the fault feature. The energy entropy extracted by VMD in four different statuses is input into the trained fault diagnosis model. Fig. 13 shows that the optimal parameters g and C are 67.12 and 72.64, respectively. It can be seen from Fig. 13 that the VNWOA-LSSVM diagnosis method has few iterations, and the fitness value can reach 0.97 after approximately 5 iterations.

The trained fault diagnosis model is applied to fault diagnosis of rolling bearings. Fig. 14 is the result of the confusion matrix using the GA-VMD-VNWOA-LSSVM method under the four different fault status. There are three misclassified samples, and the final identification accuracy rate of the

TABLE 5. VMD energy entropy under different fault statuses.

Bearing status	Feature vector (Energy entropy)						Category label
	IMF1	IMF2	IMF3	IMF4	IMF5	IMF6	
Normal	0.3676	0.20986	0.3653	0.3196	0.1015	0.0062	1
Inner ring 1	0.2516	0.2336	0.3077	0.1021	0.3198	0.3060	2
Inner ring 2	0.1575	0.1189	0.1416	0.3507	0.3529	0.2185	3
Inner ring 3	0.1742	0.0578	0.2450	0.2695	0.3637	0.2635	4
Inner ring 1	0.0579	0.0627	0.3393	0.3459	0.2142	0.2695	5
Inner ring 2	0.2383	0.3378	0.1734	0.1552	0.3207	0.1704	6
Inner ring 3	0.2141	0.1109	0.2099	0.3003	0.3648	0.3596	7
Rolling element 1	0.1151	0.1703	0.1337	0.3273	0.3469	0.2595	8
Rolling element 2	0.3362	0.1536	0.2464	0.2904	0.2847	0.2081	9
Rolling element 3	0.2766	0.2447	0.2988	0.1906	0.3242	0.2007	10

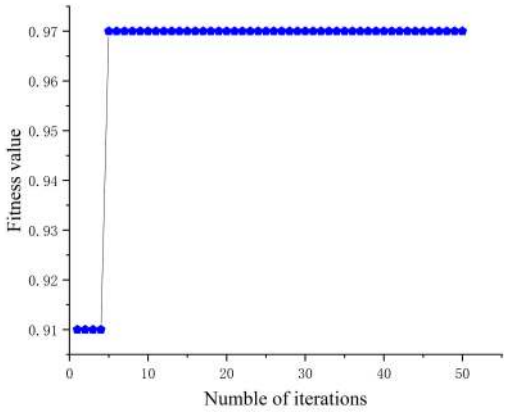

FIGURE 13. The optimal curve based on the VNWOA-LSSVM method.

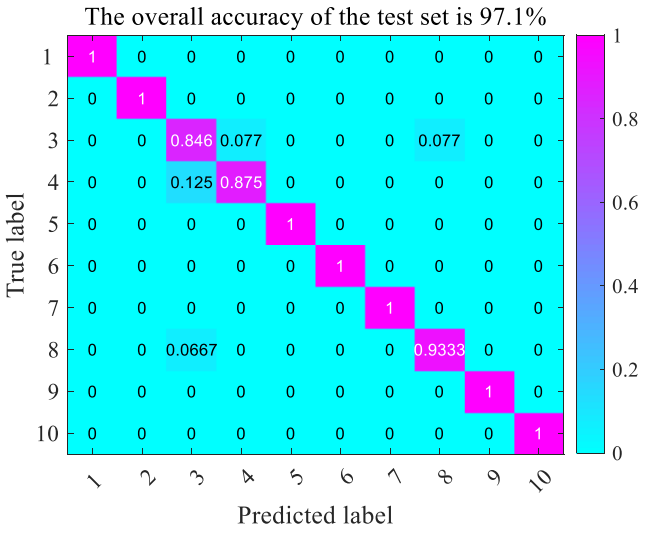

FIGURE 14. Confusion matrix of the GA-VMD-VNWOA-LSSVM method.

test set is 97.10%. The results show that this proposed fault diagnosis method can accurately identify the rolling bearing faults with different statuses.

To verify the effectiveness of this improved VMD algorithm, fault diagnosis with the improved VMD and the unoptimized VMD are conducted and compared in this manuscript. Here, the VMD parameter k is set to 6, and α is set to 2000. Fig. 15 is the result of the confusion matrix using the VMD-LSSVM fault diagnosis method, the accuracy of the label 2 is the lowest as 41.67% and the accuracy of the test set is 82.00%. Fig. 16 is the result of the confusion matrix using the VMD-VNWOA-LSSVM fault diagnosis method, and the accuracy of the test set is 83.00%. By comparing Figs.14 and 15, it can be seen that the diagnosis effect of using the improved VMD is better than that of the unoptimized VMD method, which indicates the optimized VMD can more accurately extract the fault feature information of the rolling bearing. In addition, by comparing Figs.15 and 16, it can be seen that the diagnosis effect of using the VMD-VNWOA-LSSVM is better than that of using the VMD-LSSVM method, which indicates that the VNWOA has a better optimization effect than the WOA method.

TABLE 6. Comparison data of the comprehensive performance using different methods.

Fault diagnosis method	Fitness value	Training accuracy (%)	Test accuracy (%)
VMD-LSSVM	-	91.58	83.00
GA-VMD-LSSVM	-	95.79	90.00
VMD-VNWOA-LSSVM	0.84	92.11	84.00
GA-VMD-GA-LSSVM	0.93	96.11	93.46
GA-VMD-PSO-LSSVM	0.95	98.95	95.04
GA-VMD-VNWOA-LSSVM	0.97	99.47	97.00

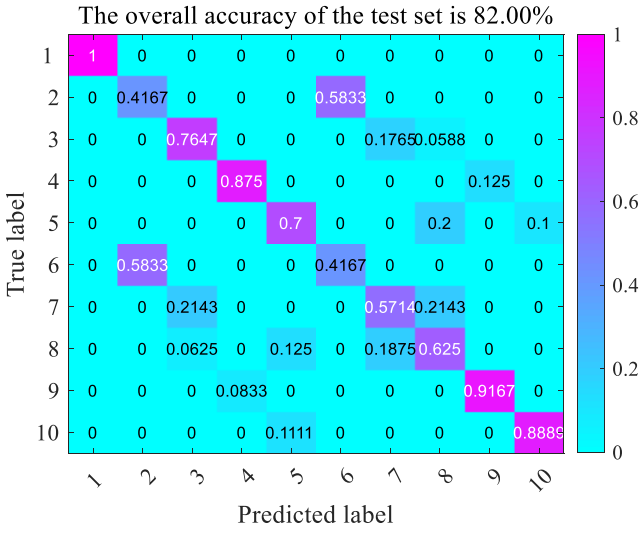

FIGURE 15. Confusion matrix of the VMD-LSSVM method.

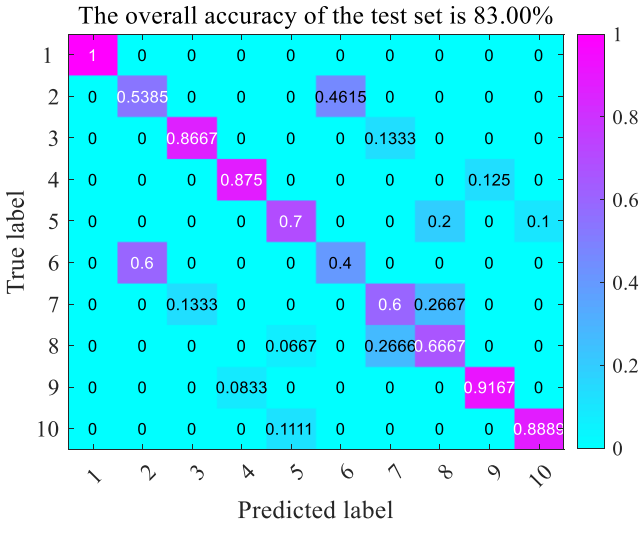

FIGURE 16. Confusion matrix of the VMD-VNWOA-LSSVM method.

Table 6 lists the fault diagnosis results using various methods such as VMD-LSSVM, GA-VMD-LSSVM, VMD-VNWOA-LSSVM, GA-VMD-GA-LSSVM, GA-VMD-PSO-LSSVM and GA-VMD-VNWOA-LSSVM. To obtain more accurate results, the data are the average values of 10 times random tests results. It can be seen from table 6 that the training and test accuracies of this proposed method are superior to those of other methods, which verifies the correctness and effectiveness of the method proposed in this manuscript.

IV. CONCLUSION

In this manuscript, a rolling bearing fault diagnosis method combining wavelet threshold de-noising, the GA-VMD energy entropy and the VNWOA-LSSVM algorithm is proposed. Fault diagnosis of a rolling bearing is conducted and analyzed from the aspects of data processing, fault feature extraction and fault feature identification. Finally, the correctness and effectiveness of the proposed method are verified.

(1) For the VMD parameter selection, the GA is utilized to obtain the best parameters, and then the optimized VMD method is adopted to extract the fault feature information after de-noising. The results show that GA-VMD can effectively extract the fault information of rolling bearings.

(2) For the parameter optimization of the penalty factor C and kernel function g in the LSSVM fault diagnosis model, the parameters are optimized by using the VNWOA method. The results indicate that the VNWOA-LSSVM method has a good searching ability, and its average diagnostic accuracy can reach 97.00%.

(3) After combining wavelet threshold de-noising, the GA-VMD energy entropy, and the VNWOA-LSSVM algorithm, fault diagnosis of rolling bearings is carried out, and the effectiveness and accuracy of the proposed method are verified through experiments. By comparing its results with those of other methods, it can be seen that the proposed method can effectively diagnose various positions and extents of the damage to rolling bearings, and it has better identification accuracy.

REFERENCES

[1] H. Lin, F. Wu, and G. He, "Rolling bearing fault diagnosis using impulse feature enhancement and nonconvex regularization," *Mech. Syst. Signal Process.*, vol. 142, Aug. 2020, Art. no. 106790.

[2] M. Kang, J. Kim, and J.-M. Kim, "Reliable fault diagnosis for incipient low-speed bearings using fault feature analysis based on a binary bat algorithm," *Inf. Sci.*, vol. 294, pp. 423–438, Feb. 2015.
[3] R. G. González-Acuña and J. C. Gutiérrez-Vega, "A transition integral transform obtained from generalization of the Fourier transform," *Ain Shams Eng. J.*, vol. 10, no. 4, pp. 841–845, Dec. 2019.
[4] H. Boche and V. Pohl, "Limits of calculating the finite Hilbert transform from discrete samples," *Appl. Comput. Harmon. Anal.*, vol. 46, no. 1, pp. 66–93, Jan. 2019.
[5] N. E. Huang, Z. Shen, S. R. Long, M. C. Wu, H. H. Shih, Q. Zheng, N.-C. Yen, C. C. Tung, and H. H. Liu, "The empirical mode decomposition and the Hilbert spectrum for nonlinear and non-stationary time series analysis," *Proc. Roy. Soc. London. A, Math., Phys. Eng. Sci.*, vol. 454, no. 1971, pp. 903–995, Mar. 1998.
[6] D. Yu, J. Cheng, and Y. Yang, "Application of EMD method and Hilbert spectrum to the fault diagnosis of roller bearings," *Mech. Syst. Signal Process.*, vol. 19, no. 2, pp. 259–270, Mar. 2005.
[7] J. Ben Ali, N. Fnaiech, L. Saidi, B. Chebel-Morello, and F. Fnaiech, "Application of empirical mode decomposition and artificial neural network for automatic bearing fault diagnosis based on vibration signals," *Appl. Acoust.*, vol. 89, pp. 16–27, Mar. 2015.
[8] G. Cai, C. Yang, Y. Pan, and J. Lv, "EMD and GNN-AdaBoost fault diagnosis for urban rail train rolling bearings," *Discrete Continuous Dyn. Syst.-S*, vol. 12, nos. 4–5, pp. 1471–1487, 2019.
[9] R. Abdelkader, A. Kaddour, A. Bendiabdellah, and Z. Derouiche, "Rolling bearing fault diagnosis based on an improved denoising method using the complete ensemble empirical mode decomposition and the optimized thresholding operation," *IEEE Sensors J.*, vol. 18, no. 17, pp. 7166–7172, Sep. 2018.
[10] Q. Xiong, Y. Xu, Y. Peng, W. Zhang, Y. Li, and L. Tang, "Low-speed rolling bearing fault diagnosis based on EMD denoising and parameter estimate with alpha stable distribution," *J. Mech. Sci. Technol.*, vol. 31, no. 4, pp. 1587–1601, Apr. 2017.
[11] C. Lv, J. Zhao, C. Wu, T. Guo, and H. Chen, "Optimization of the end effect of Hilbert-huang transform (HHT)," *Chin. J. Mech. Eng.*, vol. 30, no. 3, pp. 732–745, May 2017.
[12] S. Gaci, "A new ensemble empirical mode decomposition (EEMD) denoising method for seismic signals," *Energy Procedia*, vol. 97, pp. 84–91, Nov. 2016.
[13] J. Yang, D. Huang, D. Zhou, and H. Liu, "Optimal IMF selection and unknown fault feature extraction for rolling bearings with different defect modes," *Measurement*, vol. 157, Jun. 2020, Art. no. 107660.
[14] P. Zou, B. Hou, J. Lei, and Z. Zhang, "Bearing fault diagnosis method based on EEMD and LSTM," *Int. J. Comput. Commun. Control*, vol. 15, no. 1, Feb. 2020, Art. no. 3780.
[15] J. Sun, H. Li, and B. Xu, "Degradation feature extraction of the hydraulic pump based on high-frequency harmonic local characteristic-scale decomposition sub-signal separation and discrete cosine transform high-order singular entropy," *Adv. Mech. Eng.*, vol. 8, no. 7, Jul. 2016, Art. no. 168781401665960.
[16] Z. Tian, H. Li, and J. Sun, "Degradation feature extraction of the hydraulic pump based on local characteristic-scale decomposition and multi-fractal spectrum," *Adv. Mech. Eng.*, vol. 8, no. 11, Nov. 2016, Art. no. 1687814016676679.
[17] S. Luo, J. Cheng, and K. Wei, "A fault diagnosis model based on LCD-SVD-ANN-MIV and VPMCD for rotating machinery," *Shock Vib.*, vol. 2016, pp. 1–10, 2016.
[18] H. Ao, J. Cheng, K. Li, and T. K. Truong, "A roller bearing fault diagnosis method based on LCD energy entropy and ACROA-SVM," *Shock Vib.*, vol. 2014, pp. 1–12, 2014.
[19] K. Dragomiretskiy and D. Zosso, "Variational mode decomposition," *IEEE Trans. Signal Process.*, vol. 62, no. 3, pp. 531–544, Feb. 2014.
[20] T. Wu, C. C. Liu, and C. He, "Fault diagnosis of bearings based on KJADE and VNWOA-LSSVM algorithm," *Math. Problems Eng.*, vol. 2019, pp. 1–19, Dec. 2019.
[21] H. Ren, W. Liu, M. Shan, and X. Wang, "A new wind turbine health condition monitoring method based on VMD-MPE and feature-based transfer learning," *Measurement*, vol. 148, Dec. 2019, Art. no. 106906.
[22] R. Gu, J. Chen, R. Hong, H. Wang, and W. Wu, "Incipient fault diagnosis of rolling bearings based on adaptive variational mode decomposition and teager energy operator," *Measurement*, vol. 149, Jan. 2020, Art. no. 106941.
[23] H. Li, T. Liu, X. Wu, and Q. Chen, "Application of optimized variational mode decomposition based on kurtosis and resonance frequency in bearing fault feature extraction," *Trans. Inst. Meas. Control*, vol. 42, no. 3, pp. 518–527, Feb. 2020.
[24] Z. Wu, T. Wang, and Q. Zhang, "Research on generating detector algorithm in fault detection," in *Proc. 2nd Int. Conf. Softw. Eng. Data Mining*, Jun. 2010, pp. 23–26.
[25] C. Castejón, O. Lara, and J. C. García-Prada, "Automated diagnosis of rolling bearings using MRA and neural networks," *Mech. Syst. Signal Process.*, vol. 24, no. 1, pp. 289–299, Jan. 2010.
[26] Y. Zhang, "Fault detection and diagnosis of nonlinear processes using improved kernel independent component analysis (KICA) and support vector machine (SVM)," *Ind. Eng. Chem. Res.*, vol. 47, no. 18, pp. 6961–6971, Sep. 2008.
[27] A. Rojas and A. K. Nandi, "Practical scheme for fast detection and classification of rolling-element bearing faults using support vector machines," *Mech. Syst. Signal Process.*, vol. 20, no. 7, pp. 1523–1536, Oct. 2006.
[28] J. Wang, Z. Mo, H. Zhang, and Q. Miao, "A deep learning method for bearing fault diagnosis based on time-frequency image," *IEEE Access*, vol. 7, pp. 42373–42383, 2019.
[29] H. Ocak and K. A. Loparo, "HMM-based fault detection and diagnosis scheme for rolling element bearings," *J. Vib. Acoust.*, vol. 127, no. 4, pp. 299–306, Aug. 2005.
[30] M. M. M. Islam and J.-M. Kim, "Automated bearing fault diagnosis scheme using 2D representation of wavelet packet transform and deep convolutional neural network," *Comput. Ind.*, vol. 106, pp. 142–153, Apr. 2019.
[31] Y. Li, L. Zou, L. Jiang, and X. Zhou, "Fault diagnosis of rotating machinery based on combination of deep belief network and one-dimensional convolutional neural network," *IEEE Access*, vol. 7, pp. 165710–165723, 2019.
[32] H. Duan, Z. Li, B. Wang, R. K. Mehra, S. Luo, C. Xu, B. Sun, X. Wang, and F. Ma, "Experimental study of premixed hydrogen enriched natural gas under an alternating-current (AC) electric field and application of support vector machine (SVM) on electric field assisted combustion," *Fuel*, vol. 258, Dec. 2019, Art. no. 115934.
[33] Z. Wang, L. Yao, and Y. Cai, "Rolling bearing fault diagnosis using generalized refined composite multiscale sample entropy and optimized support vector machine," *Measurement*, vol. 156, May 2020, Art. no. 107574.
[34] Z. Qiao, Y. Liu, and Y. Liao, "An improved method of EWT and its application in rolling bearings fault diagnosis," *Shock Vib.*, vol. 2020, Mar. 2020, Art. no. 4973941.
[35] R. Vijayanand and D. Devaraj, "A novel feature selection method using whale optimization algorithm and genetic operators for intrusion detection system in wireless mesh network," *IEEE Access*, vol. 8, pp. 56847–56854, 2020.
[36] Q. Zhang and L. Liu, "Whale optimization algorithm based on lamarckian learning for global optimization problems," *IEEE Access*, vol. 7, pp. 36642–36666, 2019.
[37] X. Gao, H. Wei, T. Li, and G. Yang, "A rolling bearing fault diagnosis method based on LSSVM," *Adv. Mech. Eng.*, vol. 12, no. 1, Jan. 2020, Art. no. 168781401989956.
[38] F. Liu, J. Gao, and H. Liu, "A fault diagnosis solution of rolling bearing based on MEEMD and QPSO-LSSVM," *IEEE Access*, vol. 8, pp. 101476–101488, 2020.
[39] Y. Pan, L. Zhang, X. Wu, K. Zhang, and M. J. Skibniewski, "Structural health monitoring and assessment using wavelet packet energy spectrum," *Saf. Sci.*, vol. 120, pp. 652–665, Dec. 2019.
[40] A. G. Y. Bonda, B. K. Nanda, and S. Jonnalagadda, "Vibration signature based stability studies in internal turning with a wavelet denoising preprocessor," *Measurement*, vol. 154, Mar. 2020, Art. no. 107520.
[41] J. Chen, X. Li, M. A. Mohamed, and T. Jin, "An adaptive matrix pencil algorithm based-wavelet soft-threshold denoising for analysis of low frequency oscillation in power systems," *IEEE Access*, vol. 8, pp. 7244–7255, 2020.
[42] L. Wang, Q. Guo, Y. Liu, Y. Sun, and Z. Wei, "Contextual building selection based on a genetic algorithm in map generalization," *ISPRS Int. J. Geo-Inf.*, vol. 6, no. 9, p. 271, Aug. 2017.
[43] F. Rivas-Davalos and M. R. Irving, "An efficient genetic algorithm for optimal large-scale power distribution network planning," in *Proc. IEEE Bologna Power Tech Conf.*, Bologna, Italy, Jun. 2003, p. 5.
[44] H. Yu and Y. Shangguan, "Settlement prediction of road soft foundation using a support vector machine (SVM) based on measured data," in *Proc. MATEC Web Conf.*, vol. 67, 2016, p. 07001.

[45] S. Mirjalili and A. Lewis, "The whale optimization algorithm," *Adv. Eng. Softw.*, vol. 95, no. 5, pp. 51–67, May 2016.
[46] Y. Wang, S. Kang, Y. Jiang, G. Yang, L. Song, and V. I. Mikulovich, "Classification of fault location and the degree of performance degradation of a rolling bearing based on an improved hyper-sphere-structured multi-class support vector machine," *Mech. Syst. Signal Process.*, vol. 29, pp. 404–414, May 2012.

JUNNING LI received the Ph.D. degree from Xi'an Jiaotong University, China, in 2014. He is currently an Associate Professor with Xi'an Technological University, China. His current research interests include tribology, contact mechanics of coatings, material wear, bearing analysis, dynamics, vibration, and control.

WUGE CHEN received the B.E. degree from Xi'an Technological University, in 2018, where he is currently pursuing the M.E. degree. His current research interests include signal processing and fault diagnosis and identification.

KA HAN received the B.E. degree from Xi'an Technological University, in 2018, where he is currently pursuing the M.E. degree. His current research interests include tribology and hybrid ceramic bearing.

QIAN WANG received the B.E. degree from the Shanxi Institute of Technology, in 2018. She is currently pursuing the M.S. degree with Xi'an Technological University. Her current research interests include tribology and mechanical dynamics.